Surface acoustic wave enhanced water splitting reaction with methanol as a sacrificial material

Sixuan Wang, Rudolf Herrmann, Alexander Reiner, Achim Wixforth, Christoph Westerhausen

Angaben zur Veröffentlichung / Publication details:

Wang, Sixuan, Rudolf Herrmann, Alexander Reiner, Achim Wixforth, and Christoph Westerhausen. 2021. "Surface acoustic wave enhanced water splitting reaction with methanol as a sacrificial material." Catalysis Science & Technology 11 (4): 1458–66. https://doi.org/10.1039/d0cy01788d.

Surface acoustic wave enhanced water splitting reaction with methanol as sacrifice material†

Sixuan Wang[a], Rudolf Herrmann[a], Alexander Reiner[a], Achim Wixforth [a,b] and Christoph Westerhausen [a,b,c]

TiO_2 is the most widely used photocatalyst for water splitting reaction to generate clean fuel of hydrogen, but the energy conversion efficiency of it is still low, mainly due to the easy recombination of photo-generated electron-hole pairs. In order to promote the efficiency of the catalyst, a Surface Acoustic Waves assisted catalyst is presented in this study. On 128° rot y-cut $LiNbO_3$ Rayleigh waves with a frequency of 150MHz are generated and act on Pt modified TiO_2 catalyst nanoparticles. We here quantify the effect of the application of Surface Acoustic Waves to a Pt/TiO_2 catalyst for the hydrogen production by photo-splitting of a methanol/water vapor mixture. The results convincingly show that the photocatalytic activity of Pt/TiO_2 is clearly enhanced by the SAW propagation underneath the catalyst layer. The effect increases nonlinearly with applied power level of the acoustic wave. As the main mechanism we identify the electric field produced by the displacement of the $LiNbO_3$, which hinders the recombination of photo-generated electron-hole pairs.

Introduction

The term "photocatalysis" describes a process in which solar energy is converted into chemical energy, in most cases via a suitable (semiconductor) catalyst. Such solar-to-chemical conversion possibly represents a potential solution for any fossil fuel energy crisis and an effective strategy for environment remediation. TiO_2 is a kind of widely used and quite well understood semiconductor catalyst for photochemical reactions, for instance for the production of hydrogen from water splitting and also for degrading organic waste pollutant. However, there are some drawbacks of its photocatalytic properties due to its low efficiency of light adsorption, the fast charge carrier recombination and the slow surface redox reaction rate[1,2]. Therefore, much effort has been devoted to improve its photocatalytic efficiency to reach the demands for commercialization. In general, this comprises expansion of the TiO_2 light adsorption into the visible spectrum, improving the charge carrier separation and lowering the overpotential for surface chemical reactions. Among others, the prolongation of the charge carrier lifetime by efficiently preventing electron hole recombination remains the most critical issue. In order to obtain longer lifetimes of the charge carriers in semiconductors, various heterostructures have been constructed, such as p-n junctions[3], Schottky junctions[4] and z-scheme heterostructures[5]. The key point for these heterostructures is their built-in electric field at the material interface, which enhances the charge carrier separation and thus hinders their recombination. However, these heterostructures have to be specifically designed and synthesized for any different semiconductor and for any different photocatalytic application, which might potentially lead to high costs.

In order to reduce the cost, many research projects attempt to apply controllable external electric fields to photocatalysts, for instance, there is a growing body of work, which focuses on controlling the photochemical reaction by employing the polarization of ferroelectric materials. Ferroelectric materials have a non-centrosymmetric crystal structure, which leads to charge separation and thus polarization by supplying an external force. Many studies have shown before that this polarization can in fact enhance the separation of photo-induced charge carriers in a photocatalyst and to a promotion of surface chemical reactions. Rohrer and coworkers for example reported on a heterostructure photocatalyst comprising of a ferroelectric core ($PbTiO_3$) and a non-ferroelectric TiO_2 shell.[6] They showed that the degradation rate for methylene blue by using such a $PbTiO_3$-TiO_2 heterostructure catalyst turns out to be about five times faster than $PbTiO_3$ or TiO_2 alone and any mixture of both. They reason that this enhancement of the catalytic effect is due to the ferroelectric polarization, which causes a significant band bending at the interface between the ferroelectric and the photo-catalyst. This band bending in turn enhances the separation of photo-excited electrons and holes.

A similar work on the piezo- and also ferroelectric materials $LiNbO_3$ and $LiTaO_3$ combined with the TiO_2 photocatalyst was pioneered by Inoue and coworkers in the 1980s.[7] In their experiment, they employed conventional Pt loaded TiO_2 for a water splitting reaction, and by determining the amount of produced hydrogen, they found that the activity for the

[a] Experimental Physics I, Institute of Physics, University of Augsburg, Germany
[b] Center for NanoScience (CeNS), Ludwig-Maximilian-University, Germany
[c] Physiology, Institute of Theoretical Medicine, University of Augsburg, Germany
†Electronic Supplementary Information (ESI) available: See
DOI: 10.1039/x0xx00000x

following different material and polarization combinations turned out to be ranked like: $LiNbO_3$(negative polar surface)/TiO_2 > $LiNbO_3$(positive polar surface)/TiO_2 > $LiTaO_3$ (parallel polar surface)/TiO_2 > α-Al_2O_3(nonpolar surface)/TiO_2. The promoted catalytic activity was obviously not only due to polarization induced band bending in TiO_2, but also due to the influence on the adsorption of H_2 and O_2 on catalyst's surface.

After the discovery that static surface polarizations quite strongly affect the catalyst action on ferroelectric materials, also dynamic surface polarizations like those being produced by Surface Acoustic Waves (SAW) on piezoelectric materials have attracted attention in recent years. SAW have been long used in radio frequency (rf) telecommunications, as they represent very powerful filters and signal processing devices. They are modes of elastic energy being localized at the surface of an infinite half space substrate. SAW can be easily excited and then propagate on piezoelectric crystals, and their frequency and vibration mode can be precisely designed and controlled. Application of an rf voltage to so-called interdigital transducers (IDT) leads to the generation of an acoustic wave at a frequency and wavelength being determined by the geometry of the IDT and the SAW velocity of the respective substrate. They propagate at the speed of sound and are accompanied by the piezoelectric fields being produced by the local surface deformations of the wave. Since the surface acoustic waves hence not only provide well defined displacements of any surface volume element but they are also accompanied by strong electric fields, also propagating at the speed of sound, they provide a spatio-temporal surface polarization. However, this continuously varying system is different from the above mentioned static polarization, which could prevent the surface form achieving thermodynamic equilibrium with its environment[8]. On the other hand, also the SAW induced surface periodic spatial temporal deformations also could positively impact the activity of surface mounted catalysts, as these rapid deformations might also affect both adsorption and desorption of reactant on the catalyst surface[9,10]. It is thus expected that the SAW driven time-dependent alternating polarization in fact can more efficiently activate surface mounted catalysts.

In this work, we carry out SAW mediated catalytic water splitting reaction with methanol as hole scavenger, and employ the Pt modified titanium dioxide nanoparticles as the photocatalyst. In summary, the presented study is carried out as outlined in the following section.

Here the non-oxidative dehydrogenation of the alcohol in the methanol – water mixture is employed to produce formaldehyde and hydrogen gas. At the first photocatalytic reaction step, methanol first strongly adsorbs on the surface of TiO_2 to form methoxy species, and then the methoxy species directly react with light excited holes and decompose as follows[11]:

$$CH_3O^-(ad) + h^+ \rightarrow CH_3O\cdot(a) \quad (1)$$

$$CH_3O\cdot(a) \rightarrow CH_2O^{\cdot -}(a) + H^+ \quad (2)$$

$$CH_2O^{\cdot -}(a) \rightarrow CH_2O(a) + e^- \quad (3)$$

The anaerobic flow-conditions and the extremely small amount of catalyst in the experiment can prevent further oxidation of formaldehyde, so it is assumed that formaldehyde is the main product in the photodehydrogenation of methanol.

On the other hand, photo-excited electrons in TiO_2 are transferred to Pt, which act as active sites for hydrogen production.[12]

$$H^+(a) + e_{tr}{}^- \rightarrow \frac{1}{2}H_2(g) \quad (4)$$

By measuring the amount of photocatalytically produced formaldehyde, being proportional to the amount of H_2 produced in the catalytic water splitting process, information about the photocatalytic activity of Pt/TiO_2 can be obtained.

The SAW chip comprising an interdigital transducer IDT for the generation of surface acoustic waves[13] with a resonance frequency around f=150.3MHz was fabricated using standard microlithography. The Pt modified titanium dioxide nanoparticles serving as the photocatalyst were synthesized by a reduction method[14], and then deposited within the propagation path of the surface acoustic wave by a simple spin coating method.

This SAW based catalyst was used with and without the assistance of the Rayleigh type surface acoustic waves, and the catalytic efficacy was determined by measuring the amount of produced formaldehyde. This is achieved by applying a Hantzsch reaction of acetoacetanilide with formaldehyde and fluorometric measurements[15]. Our experimental results convincingly show that the photocatalytic activity of Pt/TiO_2 is clearly enhanced by applying an intense surface acoustic wave to it and exhibits a nonlinear relationship with the SAW power. To clarify the physical origin of the observed SAW enhancement of the catalytic efficacy, we have to consider the (i) mechanical surface deformation and (ii) the piezoelectric fields accompanying the SAW. In order to study the effect of any electric fields, we separate the catalyst layer from the piezoelectric SAW substrate by a very thin (60 nm) conductive metal film. This conductive layer is known to very efficiently attenuate the SAW induced electric fields but does not affect the SAW-induced mechanic vibration. Same photocatalysis experiments were carried out again by using this metalized SAW based catalyst. All other experimental parameters have been kept the same as in the "mechanical plus electric field" studies before. Our findings indicate that the catalysis -promoting effect of the SAW clearly decreases, when the surface electric field is attenuated.

Experimental

General procedure for synthesis of Pt modified TiO_2

To synthesize the Pt modified TiO_2 nanoparticle, we deposited Platinum nanoparticles on the surface of TiO_2 powder by a reduction method[14]. The TiO_2 powder [Degussa (P25, anatase 78%)] was used without any pretreatment. 30mg TiO_2 was suspended in 5mL, 0.4M K_2PtCl_4 solution and then stirred vigorously for 8 hours at room temperature. Thereafter, 5mg KBH_4 were gradually added to the slur. After sufficient stirring, the suspension was centrifuged and washed with pure water for 3 times. Afterwards, the sediment was dried and we put 20mg produced Pt/TiO_2 into 1mL ethanol to obtain the suspension

used for spin coating. All the chemicals were purchased from Sigma Aldrich. Finally, the synthesized Pt modified TiO_2 was inspected with a scanning electron microscope (SEM) to check their morphology as shown in Fig.1(c_1) and (c_2).

Design and fabrication of the SAW chips

For the SAW chips, we used 128° rotated Y-cut $LiNbO_3$ single crystal substrates, on which Rayleigh type SAW are generated. The size of the $LiNbO_3$ chips is 17.5mm×17.5mm and the thickness of the chip is 0.5mm. The designed IDT had an aperture of W=2mm and a finger spacing of d=6.25µm, which results in a SAW wavelength of λ=25µm. The IDT employed had 16 finger pairs. These IDT were micro lithographically fabricated near the sides of the substrate, and consisted of 5nm Ti on the bottom, then 50nm Au and 5nm Ti on the top. Lastly, a h=100nm thick SiO_2 layer was deposited on top of the whole $LiNbO_3$ substrate by thermal evaporation, serving as a protection film. After fabrication, the resonance frequency and the return loss S_{11} of the IDT was determined by a vector network analyzer (Rohde & Schwarz).

SAW-based Pt/TiO_2 catalyst chip

To finalize the SAW assisted catalysis samples, we spin coated (1500rpm for 5 seconds) 8µL Pt/TiO_2-ethanol suspension of the Pt/TiO_2 catalyst directly onto the propagation path of the $LiNbO_3$ SAW delay lines. Then, this coated substrate was baked at T=80°C for 5min to evaporate all ethanol. Finally, any accidentally deposited catalyst layer outside the SAW propagation path was carefully removed to ensure that all the present catalyst particles are influenced by the SAW. This resulted in an active catalyst area of around 2mm×8mm. The side view of the SAW-based Pt/TiO_2 catalyst chip is shown in Fig. 1(b_1). The morphology of the catalyst films was measured with an AFM and the thickness of the film was checked by Dektak© profilometer, and the results of both are presented show in Fig. 1(d) and (e).

To characterize the SAW chip and to check whether the thin catalyst layer possibly alters the SAW propagation mode, we manufactured two otherwise nominally identical SAW delay lines with and without the thin catalyst layer and compared their rf transmission functions employing a network analyzer. The measured S_{21} transmission in the time domain shows that the catalyst layer does not affect the SAW propagation mode once being deposited on the chip, except for a 10dB attenuation of the transmitted signal (see supplementary information).

Determine the amount of the formaldehyde

The quantity of the produced formaldehyde is determined by a Hantzsch reaction of acetoacetanilide (AAA) with formaldehyde which involves a cyclization between AAA and formaldehyde in the presence of ammonia so that it will produce a yellow dihydropyridine derivative product which in turn can be detected in a fluorometric measurement with λ=370nm excitation[15]. This method is very simple and sensitive, and allows the measurement of formaldehyde at the µmol·L^{-1} level. In addition, the Hantzsch reaction can take place at room temperature without any heating system.

For calibration purposes, a series of formaldehyde standard solutions was prepared which has concentrations of 0, 0.856µmol·l^{-1}, 1.712µmol·l^{-1}, and 2.569µmol·l^{-1}. After 30minutes Hantzsch reaction, the solutions were spectroscopically measured at room temperature, which allows the preparation of a calibration graph. Fig. 2(a) illustrates that the emission intensity at 472nm increases with the HCHO concentrations, in a range of 0 - 2.5µmol·l^{-1}, and according to Li's work, the lowest determined level is 0.1µmol·l^{-1} [15]. Fig. 2(b) shows the clear linear correlation between formaldehyde concentration and fluorescence intensity (linear regression: $y = 17630.8x + 41771.9$, correlation coefficient 0.9974, x =[HCHO] in µmol·l^{-1}, y = fluorescence intensity).

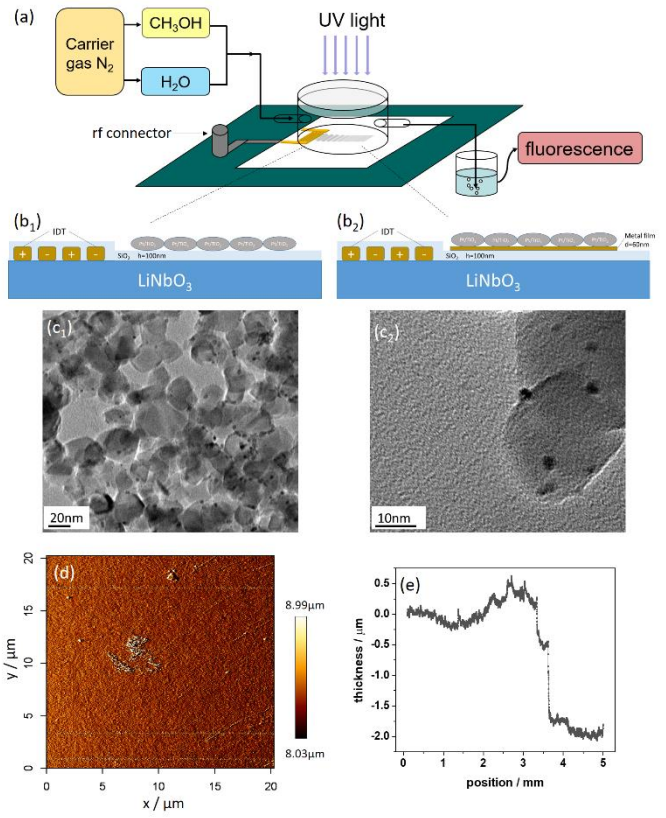

Fig. 1 (a) the setup: The green part represents a circuit board which holds an rf connector, the SAW chip with the catalyst layer in the propagation path of a surface acoustic wave and the micro reaction chamber. Through a quartz glass window on top of the cylinder the sample is illuminated with UV radiation. The reaction chamber has a gas inlet and a gas outlet. The inlet is supplied with nitrogen, water and methanol vapor, and the outlet may in addition contain hydrogen and formaldehyde, the latter serving as an indicator for the hard detectable H_2. (b_1) represents the SAW-based Pt/TiO_2 catalyst device without metal layer, and (b_2) represents the SAW-based Pt/TiO_2 catalyst device with metal layer. (c_1) and (c_2) TEM pictures of synthesized Pt/TiO_2 catalyst. (d) represents the AFM picture of spin-coated Pt/TiO_2 catalyst film. (e) Dektak© profilometer measurement for the thickness of the catalyst film.

Acoustic-photocatalysis and its dependence on SAW power

The gas-phase catalytic reaction takes place in a flow-type reaction cell, in which a small (1cm^3) cylindrical chamber with a quartz window on top was in direct contact with the $LiNbO_3$ sample and the Pt/TiO_2 catalyst. A UV light emitting diode (λ=365nm) was placed above the reactor cell, and its irradiation intensity is P_{LED} = 85mW/cm^2 which was determined by a power meter (Thorlabs PM100A). We use nitrogen as carrier gas and it passed through liquid water and methanol at flow rates of 4.8mL/min and 0.2mL/min, respectively. Then, these gas

photocatalytic reaction cell. In Fig. 1(a), a schematic of our setup is depicted. Before the photocatalysis experiments, the reaction cell was flushed with nitrogen-water-methanol vapor for one day to reach anaerobic conditions. As reference measurement the gas mixture passed the chamber and was bubbled in an adsorption solution, which was used for the Hantzsch reaction, for 30 minutes. Its fluorescence represents the base line for the subsequent "active" measurements with UV LED and SAW for 60 min (f_{SAW} =150MHz and P_{SAW} = 40mW). During the SAW-assisted-photocatalytical process, every 30 min, the adsorption solution was exchanged by fresh one and the fluorescence emission of the previous adsorption solution was checked immediately to determine the amount of formaldehyde produced.

For comparison, reference experiments were also carried out with UV illumination only (no SAW) to be able to investigate the effect of the SAW on the photocatalytic efficiency. The results are shown in Fig. 2(c), (d) and (e). Clearly, a positive effect of the additional SAW interaction with the catalyst is seen.

To study the relationship between the applied SAW power level P_{SAW} and the enhancement of photocatalytic reaction, these photocatalytic reactions were carried out for different SAW power levels P_{SAW}=10mW, 20mW, 30mW and 40mW separately. The Pt/TiO_2 catalyst was prepared fresh after each experiment. Here the activation coefficient indicates the effect of SAW to the photocatalytic reaction. The activation coefficient is defined as AC:= M_{SAW+UV} / M_{UV}, where M_{SAW+UV} is the yield amount of formaldehyde when SAW was applied during UV illumination, and M_{UV} is the yield amount of formaldehyde when SAW was not applied during UV illumination. The result is shown in Fig.2(f).

Separation of mechanical and electric contribution to SAW effect

In order to distinguish between the mechanical vibration and the accompanying electric fields as main contribution to the enhanced photocatalysis reaction, the SAW chip was modified by a thermally deposited 60nm thick metal film, which consists of a simple metallization (5nmTi+50nmAu+5nmTi) of the SAW propagation path before we deposit the Pt/TiO_2 catalyst on it. The side view of the metalized SAW-based Pt/TiO_2 catalyst chip is shown in Fig. 1(b_2). This metallization has no significant influence on the mechanical deformation of the chip surface, because the thickness of the metal film (60nm) is much lower than the wavelength of SAW (25µm), but it can completely alter the electrical boundary conditions at the surface. A (thin and massless) conductive layer on the surface of a SAW substrate, however, efficiently shortens the piezoelectric fields accompanying the SAW and also renormalizes the SAW velocity to a somewhat lower (Δv) value as compared to the open, unmetallized surface (v_0)[16]. The same photocatalytic reaction was carried out again at the resonance frequency by using P_{SAW} =10mW, 20mW, 30mW and 40mW SAW power separately, and the obtained activation coefficient results (AC_2) were compared with the one got at same SAW power but with non-metalized SAW chip before (AC_1).

Results and discussion

Morphology of the catalyst

The two SEM images shown in Fig. 1(c_1) and (c_2) illustrate that the diameter of TiO_2 (P25) nanoparticle was around 20nm and the size of Pt nanoparticle was around 1nm in diameter, and these Pt nanoparticles are located on the surface of TiO_2. The Fig. 1(d) shows that the roughness of the spin-coated catalyst film is relative small. Fig. 1(e) shows a profiolometer measurement for the determination of the thickness of the catalyst film. Here the positions from 0 to 3.5mm represent the area of the catalyst film, and 3.5mm to 5mm is the area of substrate. We find that the thickness of the film is around 2µm, which is much less than the SAW wavelength (25µm), this indicate that this catalyst film should not lead to another type of acoustic wave, which is supported by additional measurements shown in the supplementary information.

Photocatalytical reaction with the assistance of 40mW SAW

During the 60 mins photocatalytic reaction, fluorescence emission intensity of adsorption solution was checked every 30minutes. The result of pure photocatalytic reaction with only UV light is shown in Fig. 2(c), and the result of acoustic-photocatalytic reaction with assistance of 40mW SAW is shown in Fig. 2(d). As can be seen from these figures, the additional effect of the P_{SAW}=40 mW surface acoustic wave results in a clear increase of the fluorescence emission intensity after t=30 min and t= 60 min, respectively, whereas the fluorescence intensities in the dark are almost the same. Based on our calibration data as being depicted in Fig. 2(b), we can now determine the amount of formaldehyde being produced during the reaction. The data presented in Fig. 2(e) illustrate that the amount of the produced formaldehyde is about 0.008µmol after 1 hour UV illumination, and doubles to 0.016µmol when a SAW is acting additionally upon the photocatalyst. Due to the small area of catalyst film, of only 2mm×8mm, the total amount of produced formaldehyde is very small, but we still observe a nearly 100% increase of the production efficiency under P_{SAW} = 40mW SAW interaction.

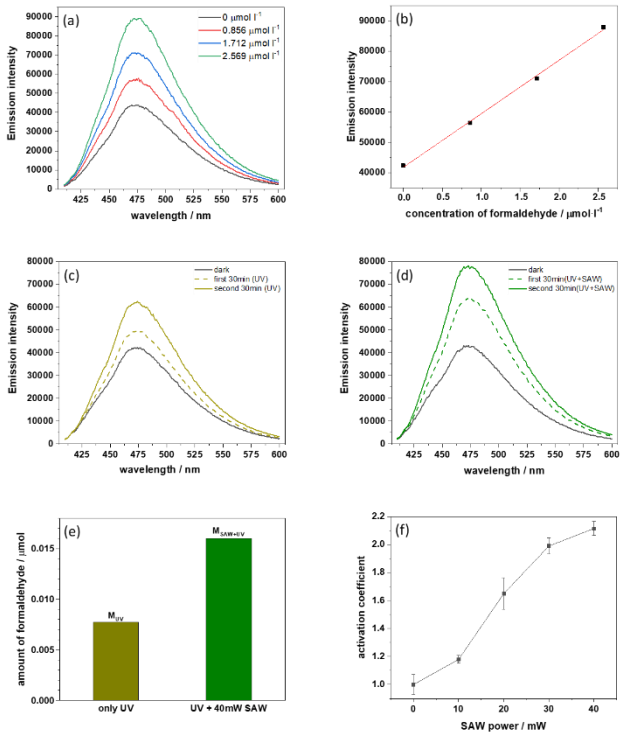

Fig. 2: (a) fluorescence emission intensity of standard formaldehyde solutions with different concentrations; (b) calibration graph of the raw data shown in (a); (c) Fluorescence emission intensity of the adsorption solution after 30minutes in the dark (black line), after first 30minutes UV illumination + no SAW (yellow dashed line), and another 30minutes UV illumination + no SAW (yellow solid line); (d) Fluorescence emission intensity of the adsorption solution, the same experiment as being depicted in (c) but with SAW on at P_{SAW} = 40mW; (e) The amount of formaldehyde being produced during the photocatalytic processes for UV illumination only and UV illumination plus P_{SAW} = 40mW SAW; (f) Activation coefficient (as being defined in the text) for various SAW power levels P_{SAW} = 0mW, 10mW, 20mW, 30mW and P_{SAW} = 40mW.

In order to exclude any spurious SAW heating effect, we monitored the temperature changes during the experiment by employing a miniature temperature sensor. The result of this control experiment is shown in the supplementary information: the total temperature (obviously mainly caused by the UV illumination) increases by about 20 K during the experiment and the P_{SAW}=40mW SAW causes only a negligible additional temperature rise. Thus, it is safe to state that the SAW, which clearly produces a doubling in the catalytic efficiency, does not act via an additional temperature increase but rather via intrinsic SAW related effects.

Figure 3 shows the return loss S11 of the chip. Due to large bandwidth of the IDT structure (≈8MHz), less than 0.1dB power change is caused by a ΔT=20°C temperature rise, as the reported temperature expansion coefficient for 128° rotated y-cut LiNbO3 is 76ppm/°C[17] and the output frequency of the rf generator was kept constant at 150.3MHz. Hence, the observed nearly 100% increase of the catalytic efficiency due to SAW interaction might even be a bit larger, taking the non-compensated shift of the SAW resonance frequency into account.

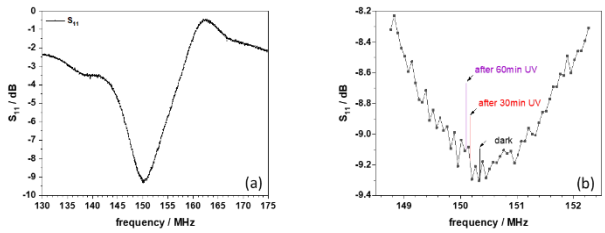

Fig. 3 Return loss S_{11}. Left: the resonance frequency of the IDT measured by a network analyzer at room temperature; right: zoom in on the left panel; after 30min and 60 min of UV illumination the resonance frequency is only slightly shifted to the values indicated by the vertical lines.

Acoustic-photocatalysis depends on SAW power

Now that it has been unambiguously shown, that the SAW increases the catalytic reaction efficiency of our assay by a non-temperature related effect, we turn to a detailed investigation of the SAW power dependence of this efficiency. In Fig. 2(f), we use the extracted activation coefficient AC= M_{SAW+UV} / M_{UV} of our reaction, where M denotes the amount of formaldehyde being detected by the fluorescence intensity measurements with and without SAW as described above. We find that the activation coefficient seems to first strongly increase and then to saturate for P_{SAW}>30mW. The increasing activation coefficient AC indicates a SAW-enhanced photocatalytic activity of Pt/TiO_2. In this experiment, SAW propagate at the surface of $LiNbO_3$, and at the same time, these waves can cause well-defined displacements at the surface of substrate, and these mechanical displacements are also accompanied by electric potential because the distorted substrate is a piezoelectric material. The spatial and temporal positive and negative surface polarization lead to a strong electric field near the surface. The SAW induced electric potential (Ø) is related to the square root of the power level of the SAW according to the equation (5). The SAW induced electric field and amplitude of the mechanic vibration are both related to the SAW induced electric potential according to the equation (6) and (7).[18]

$$_{SAW} = \frac{1}{2}\frac{A}{\lambda}\ _0|\emptyset|^2 \qquad (5)$$

Here, A is the beam width of the SAW, λ is the wavelength and $_0$ a material dependent constant ($y_{0,LiNbO_3}(128°) = 0.21mS$).

Electric field:

$$E_x = -\frac{\partial \emptyset}{\partial x} = jk\emptyset, \qquad E_y = -\frac{\partial \emptyset}{\partial y} = 0, \qquad E_z = -\frac{\partial \emptyset}{\partial z} \qquad (6)$$

Here, E_x and E_y are the SAW-induced in-plane electric field, and x is the SAW propagation direction. E_z is the out-of-plane electric field, and the z direction is perpendicular to the surface of substrate. Since the SAW is travelling along the x direction, $\partial/\partial x$ can be represented by j·k, where k is the wave vector. The in-plane electric field E_y is always zero because SAW are a kind of travelling waves and are uniform in y direction. $\partial/\partial z$ can be

represented as a sum of decaying exponentials because the SAW decays underneath the surface of substrate. Typical fields for the applied power range in this study range from E=1.65×10^5 V/m to E=3.31×10^5 V/m, while both positive and negative signs are possible.

The displacement at the surface are also related to the surface potential Ø through the piezoelectric constants c_x, c_y and c_z.

Mechanical vibration:

$$u_x = c_x \cdot \emptyset, \quad u_y = c_y \cdot \emptyset, \quad u_z = c_z \cdot \emptyset \tag{7}$$

Here u_x is the displacement along the x direction, u_y is the displacement along the y direction and u_z is the displacement along z direction.

Equations of (5) (6) and (7) indicate that the SAW-induced surface potential, electric field and mechanical vibration are positively related to the square root of the SAW power level. When the SAW power increases, these SAW-induced accompanying parameters will also increase. This gives rise to the interpretation that the SAW-induced surface deformations, electric fields and electric potential could be the reason for the SAW power depended catalytic activity.

The SAW-induced electric field could directly affect the band structure of TiO_2. As we know, TiO_2 is a semiconductor catalyst, which has a well-defined conduction band and a valence band. When it is under influence of a strong enough electric field, this external electric field could cause a certain band bending of the TiO_2. $LiNbO_3$ is a non-centro-symmetric crystal structure, so it has an internal dipole and piezoelectric effect. The internal dipole can cause electrical states of the material, while the piezoelectric effect is a linear interaction between the mechanical and electrical states in the crystal. When the SAW propagates on the $LiNbO_3$, the change of mechanical stress causes the movement of the center of negative charge and the center of positive charge, and furthermore change the internal dipole. As a consequence the surface dynamically exhibits a negative or positive surface charge upon the propagation of a piezoactive surface wave. The SAW, being responsible for a dynamic poling of the $LiNbO_3$ substrate, also couples electric fields into the Pt/TiO_2 nanoparticles where it induces a dynamical band bending and the formation of depletion and accumulation layers in the TiO_2. To illustrate this idea, we sketch in Fig. 4(a) and (b) the schematic energy level diagrams of TiO_2 under both negative and positive polarization. On positive poled $LiNbO_3$, there are many positive polarization charges at the interface of $LiNbO_3$, which causes a drift of the negative free charge carriers in the TiO_2 toward the interface to compensate the positive polarization. These redundant negative free charge carriers cause a negative charged depletion layer, and lead to downward band bending. Positive free charge carriers, on the other hand, move into the opposite direction, namely the interface between TiO_2 and gas phase, these redundant positive free charge carriers cause a positive charged depletion layer, and lead to upward band bending. As a result, the SAW-induced external electric field lead to an internal electric field at the interface of $LiNbO_3$/TiO_2 and the interface of TiO_2/gas. There, under UV light illumination, electrons are excited from the valence band of TiO_2 to the conduction band of TiO_2, and leave holes in the valence band. These photoexcited electron-hole pairs can be separated by the external SAW-induced electric filed, the photoexcited electrons in the TiO_2 move toward the $LiNbO_3$/TiO_2 interface while the photoexcited holes drift towards the TiO_2/gas interface. Moreover, the upward-bent band at the TiO_2/gas interface tends to accumulate holes at the interface, then these holes take part in the oxidation reaction. Both the CH_3OH and the H_2O could interact with these holes but most holes will react with methanol since it always serves as hole scavenger, and transient spectroscopic studies have revealed that the reaction of CH_3OH and the hole happens at a much faster rate than the one for the H_2O molecules and holes[11]. Here, the methanol does not only serve as hole scavenger, as a hydrogen-containing sacrificing material, it also contributes its hydrogen atom to produce hydrogen gas. The produced $\cdot CH_3O$ radical (see chemical reaction (1)) is an excellent electron donor[19], which dissociates a proton (reaction (2)) and injects its electron (reaction (3)) to the conduction band of TiO_2, which is called "doubling effect"[20,21]. The injected electron prefers to aggregate on the Pt nanoparticle being located at the surface of TiO_2, and it reduces the dissociated proton into hydrogen gas. Here, the Pt nanoparticle acts as an active site for the reduction reaction to produce hydrogen gas, because it can capture photogenerated electrons, and also lowers the overpotential for hydrogen production[12].

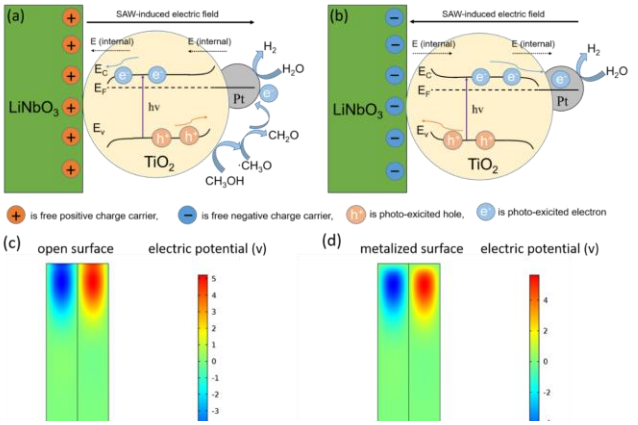

Fig. 4 Schematic energy level diagrams of TiO_2 under condition of (a) negative polarization and (b) positive polarization normal to the $LiNbO_3$/TiO_2 interface. E_C represents the conduction band edge and E_V represents the valence band edge of the TiO_2. (c) and (d) COMSOL simulated electric potential of $LiNbO_3$, the rectangle is the side view of 128° y-cut $LiNbO_3$, and the width of $LiNbO_3$ is 25μm (one wavelength) and the height is 75μm, and propagation direction of wave is along the width of the rectangle. The surface of $LiNbO_3$, where SAW propagate, is at the top of rectangle. (c) depicts the simulated electric potential when the surface is free, and (d) depicts the simulated electric potential when the surface is covered with metal.

For a temporary negatively poled $LiNbO_3$, the positive free charge carriers in TiO_2 will move toward the interface of $LiNbO_3$/TiO_2 and lead to upward band bending, at the same time, the negative free charge carrier in TiO_2 will drift to the interface of TiO_2/gas and lead to downward band bending. The

photoexcited electron-hole pairs are subsequently spatially separated by the electric field travelling with the SAW and are driven into opposite directions, the photoexcited electrons drift to the interface of TiO_2/gas, and the downward band bending help the electrons to transfer firstly to Pt nanoparticle and then take part in the reduction reaction to produce hydrogen gas. This SAW-induced electric field and caused band bending quite efficiently prevents electrons and hole recombination and leads to longer lifetimes of these charge carriers, which in turn strongly promotes the photocatalytic reaction.

On the other hand, the SAW-induced mechanical vibration could accelerate the chemical reaction by reducing the strain depended diffusion barrier of the reactant. For a heterogeneous catalysis process, the reactant is firstly adsorbed on the catalyst's surface and then diffuses to the active site of the catalyst. Secondly, the chemical reaction can take place on the active site and the adsorbed reactant changes into the product. Some detailed analysis of the SAW promoted activation at the atomic-level in surface catalytic process are done by Wu et al., and his theoretical and computational investigation illustrates that the action of Rayleigh acoustic waves could enhance the surface diffusion of adsorbed atom by tens and hundreds percent[22], which could also positively affect the activity of the catalyst.

Separation of the electric and mechanic contributions to the SAW effect on catalysis

In order to further elucidate the physical mechanism behind the observed beneficial interaction mechanism of a SAW, enhancing the efficiency of the photocatalytic reaction, the exact same photocatalytic reaction was carried out again at the SAW resonance frequency but with a metalized SAW chip, for different SAW power levels. P_{SAW}= 10mW, 20mW, 30mW and 40mW SAW were applied separately to the Pt/TiO_2 catalyst during one hour UV illumination.

The SAW-induced electric potential for the open surface and the metalized surface are simulated using COMSOL software and are shown in the Fig. 4(c) and (d) separately.

The activation coefficients AC_1 for the normal SAW chip (open surface) and AC_2 for the metallized SAW chip are compared in Fig. 5(a). Moreover, the multiplication constant for SAW-induced electric field (E_{field}), AC_1 and AC_2 for various SAW power are compared in Fig. 5(b), where the SAW-induced electric fields (E_{field}) are normalized by the E_{field} which is produced by the P_{SAW}=10mW SAW, so the multiplication constant for P_{SAW}=10mW, 20mW, 30mW and 40mW SAW-induced E_{field} are 1, $\sqrt{2}$, $\sqrt{3}$, and 2 respectively. Using the same method, all AC_1(normal SAW chip) values were also normalized to the AC_1 at P_{SAW}=10mW, and all AC_2(metalized SAW chip) values were normalized to the AC_2 for P_{SAW}=10mW SAW.

In Fig. 5(a), we can clearly see that the value of AC_1(normal SAW chip) and AC_2(metalized SAW chip) both exceed unity, when P_{SAW} = 10mW, 20mW, 30mW and 40mW SAW is applied. This experimental finding in fact reveals that obviously both the "metal film modified" SAW chip and the non-metalized "normal" SAW chip enhance the catalytic activity of Pt/TiO_2. At the same SAW power, however, the AC_2 (metalized SAW chip) are always smaller than the AC_1 (normal SAW chip). This indicates that the obvious SAW-promoted catalytic efficiency was somewhat weakened by the 60nm metal film. The metal film cancels the SAW-generated electric potential at the surface ($\emptyset = 0$), and it short circuits the in-plane electric field E_x and E_y, which are parallel to the surface of substrate, The out-of-plane electric field E_z, which is perpendicular to the surface, is strongly reduced. In terms of mechanical vibrations, metalization is not a prominent factor, since the thickness of metal film (60nm) is much smaller than SAW wavelength (25µm) and the mass loading of such a thin film is negligible[23].

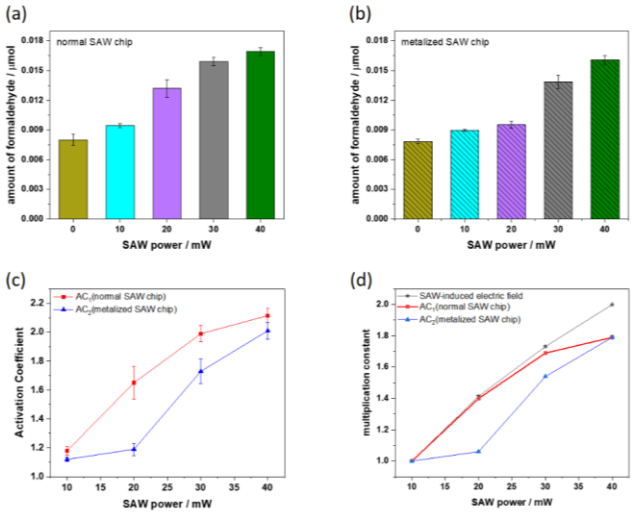

Fig. 5 Amount of produced formaldehyde as function of SAW power for the normal (a) and metalized (b) SAW chip. (c) Activation coefficient AC_1 and AC_2 for various SAW power, separately prepared sample for each power level. Resonance frequency was kept at f_{SAW} = 150.3MHz. (d) the multiplication constant for SAW-induced electric field (E_{field}), AC_1 and AC_2 for various SAW power levels.

Hence, the metalized SAW chip and the normal SAW chip basically provide the same mechanical vibration at the same SAW power. As a result, we consider the reason for the smaller AC_2 (metalized SAW chip) as compared to AC_1 (normal SAW chip) to be the SAW-induced electric field (E_{field}) although being reduced by the metal film. The reduced electric field values, however, cannot cause the same significant band bending of TiO_2. Moreover, these photo-excited electrons and holes will not be efficiently separated by the small external SAW-induced electric field (E_{field}) and most of them have a chance to recombine, thus these photocatalytic reactions are not so significantly promoted as we observe it in the experiment for the normal chip.

For the normal SAW chip, AC_1 at P_{SAW} = 10mW was AC_1=1.18, and it was AC_1=1.65 at P_{SAW} = 20mW, which is 1.4 times bigger. However, for the metalized SAW chip, AC_2 at P_{SAW} = 20mW was AC_2=1.19 and thus only 1.06 times bigger than the AC_2 at P_{SAW} = 10mW. When the power of SAW is doubled from P_{SAW} = 10mW

to 20mW, the SAW-induced mechanical vibration and electric field will become $\sqrt{2}$ times stronger, according to equations (5), (6) and (7). We know that the metal film causes only a negligible attenuation of the mechanical vibrations, so they should be increased from P_{SAW} = 10mW to P_{SAW} = 20mW the same factor for both the normal SAW chip and the metalized SAW chip. However, we observe a significantly larger SAW mediated increase for AC_1 (normal SAW chip) but not for AC_2(metalized SAW chip), so we take this fact as a signature to be safe to exclude the SAW-induced mechanical vibration as the main reason for SAW-promoted catalytic property. Again, in terms of SAW-induced electric fields (E_x, E_y and E_z), due to the shortcut and attenuation effect of the metal film, the in-plane electric field E_x=0 and E_y=0, and the out-of-plane electric field E_z(metalized SAW chip) is smaller than the E_z (normal SAW chip). Therefore, this weaker electric fields might not efficiently separate the electron-hole pair and prolong their lifetime, which might be the reason for the low AC_2 value under the influence of the P_{SAW} = 20mW SAW.

In Fig. 5(b), it is obvious that the multiplication constant of AC_1(normal SAW chip) is almost constant with the multiplication of the SAW-induced electric field when the applied SAW power is lower than 30mW. As has been analyzed above, the SAW-induced electric field is the main reason the promotion of catalytic activity, so the E_{field} and AC_1 have the same rising tendency. However, the tendency deviates when the SAW power exceed P_{SAW}=30mW, the increase of AC_1 is lower than the increase of SAW-induced E_{field}, the reason of which might be the further oxidation of formaldehyde. Even though the reaction rate of CH_3OH and the photoexcited holes is faster than the one for the H_2O molecules and holes, some hole will still inevitably react with H_2O molecule and oxidize it into free ·OH radical[19], and due to its strong oxidizing properties, the free ·OH radical could further oxidize formaldehyde into HCOOH or CO_2[24]. Under the condition of big SAW power, the SAW-induced electric field is relative strong and this can help to efficiently separate photoexcited electron-hole pairs and hinder their recombination. Even though the illumination with UV light is still the same, but the amount of photogenerated electrons and holes become bigger, the produced amount of formaldehyde and ·OH radical production also become bigger, but some amount of formaldehyde will be consumed by the oxidation of the free ·OH radical. As the result, the finally detected amount of formaldehyde is not increasing with the increase of the SAW induced electric field, explaining the differences in increase of AC_1 and the electrical field with increasing SAW power. For the metalized SAW chip, the electrical field is smaller because of the screening and attenuation effect of the metal film. At low SAW power (10mW and 20mW), the SAW-induced electric field is not strong enough to significantly separate the electron-hole pairs, so the multiplication constant of AC_2 are almost equal to 1. At high SAW power (30mW and 40mW) the electrical field becomes stronger, but still remains smaller than that caused by the non-metalized normal SAW chip at the same SAW power. Hence, the increased reaction rate is not fast enough to promote further oxidation of formaldehyde, and AC_2 exhibits the same tendency as the electrical field.

Conclusions

We have performed experiments in which Rayleigh type piezoelectric surface acoustic waves with a resonance frequency of 150MHz act upon well-known Pt/TiO_2 photocatalysts during the photocatalysis of a water splitting reaction with methanol as hole scavenger.

To quantify the SAW-enhanced catalytic efficiency, we employed a Hantzsch reaction to detect the photoexcited hole oxidized formaldehyde production. Here, acetoacetanilide (AAA) with formaldehyde in the presence of ammonia which produces a yellow dihydropyridine derivative product that can be quantitatively detected in a fluorometric measurement. Due to the "doubling effect" of methanol, we can thus approximately determine the amount of H_2 production. Our experimental findings show that the SAW in fact can improve the catalytic efficiency for the methanol photodehydrogenation and that this effect increases with increasing applied SAW power. According to the comparison experiment with a non-metalized normal SAW chip and a metalized SAW chip, we argue that the SAW accompanying electric field is most likely the reason for this enhancement. The SAW, being responsible for a dynamic poling of the $LiNbO_3$ substrate, also couples electric fields into the surface deposited Pt/TiO_2 nanoparticle where it prevents the recombination of electron-hole pairs and prolong their lifetime. Moreover, it also induces dynamical band bending of TiO_2. The longer lifetime of charge carriers and the band bending of TiO_2 finally enhance the photocatalytic reaction.

Conflicts of interest

There are no conflicts to declare

Acknowledgements

This project has received funding from the European Union's Horizon 2020 research and innovation programme under the Marie Sklodowska-Curie Grant agreement No 642688 (SAWtrain). The authors thank the Cluster of Excellence 'Nanosystems Initiative Munich (NIM)' and the 'Augsburg Centre for Innovative Technologies (ACIT)' for funding. Special thanks to Andreas Hefele, Matthias Küß, Lukas Schnitzler, and Andreas Hörner for technical assistance.

References

1 T. Hisatomi, J. Kubota, and K. Domen, *Chem. Soc. Rev.*, 2014, **43**, 7520.
2 A. Kudo and Y. Miseki, *Chem. Soc. Rev.*, 2009, **38**, 253.
3 J. Zhang, S. Z. Qiao, L. Qi, and J. Yu, *Phys Chem Chem Phys.*, 2013, **15**, 12088.
4 X. Li, H. Zhu, K. Wang, A. Cao, J. Wei, C. Li, Y. Jia, Z. Li, X. Li and D. Wu, *Adv. Mater.*, 2010, **22**, 2743.
5 P. Zhou, J. Yu and M. Jaroniec, *Adv. Mater.*, 2014, **26**, 4920.
6 L. Li, Y. Zhang, A. M. Schultz, X. Liu, P. A. Salvador and G. S. Rohrer, *Catal. Sci. Technol.*, 2012, **2**, 1945.

7 Y. Inoue, M. Okamura and K. Sato*, J. Phys. Chem.*, 1985, **89**, 5184.
8 M. B. Starr and X. Wang, *Nano Energy*, DOI:10.1016/j.nanoen.2015.01.035.
9 H. Nishiyama, N. Rattana, N. Saito, K. Sato and Y. Inoue, *J. Phys. Chem. B*, 2000, **104**, 10602.
10 H. Nishiyama, N. Saito, H. Chou, K. Sato and Y. Inoue, *Surf. Sci.*, 1999, **433-435**, 525.
11 T. Chen, Z. Feng, G. Wu, J. Shi, G. Ma, P. Ying and C. Li, *J. Phys. Chem. C*, 2007, **111**, 8005.
12 Q. Hao, Zhiqiangwang, T. Wang, Z. Ren, C. Zhou and X. Yang, ACS Catal., 2019, **9**, 286.
13 R. M. White and F. W. Voltmer, *Appl. Phys. Lett.*, 1965, **7**, 314.
14 Torrano, A. A., Herrmann, R., Strobel, C., Rennhak, M., Engelke, H., Reller, A., ... & Bräuchle, C. (2016). Nanoscale, 8(27), 13352-13367.
15 Q. Li, P. Sritharathikhun and S. Motomizu, *Anal. Sci.*, 2007, **23**, 413.
16 A. Wixforth, J. P. Kotthaus and G. Weimann, Phys. Rev. Lett., 1986, 56, 2104.
17 N. Dewan, M. Tomar, V. Gupta and K. Sreenivas, *Appl. Phys. Lett.*, 2005, **86**, 223508.
18 S. Datta, Surface Acoustic Wave Devices, Prentice-Hall, Englewood Cliffs, N.J., 1986.
19 F. Guzman, S. S. C. Chuang and C. Yang, *Ind. Eng. Chem. Res.*, 2013, **52**, 61.
20 N. Hykaway, W. M. Sears, H. Morisaki and S. R. Morrison, *J. Phys. Chem.*, , 1986, **90**, 6663.
21 J. Schneider and D. W. Bahnemann, *J. Phys. Chem. Lett.*, 2013, **4**, 3479.
22 C. Wu, V. Y. Zaitsev and L. V. Zhigilei, *J. Phys. Chem. C*, 2013, **117**, 9252.
23 B. Paschke, A. Wixforth, D. Denysenko and D. Volkmer, *ACS Sens.*, 2017, **2**, 740.
24 H. Sheng, Q. Li, W. Ma, H. Ji, C. Chen and J. Zhao, *Appl. Catal. B Environ.*, 2013, **138-139**, 212.

Supplementary Information to: Surface acoustic wave enhanced water splitting reaction with methanol as sacrifice material

Sixuan Wang[a], Rudolf Herrmann[a], Alexander Reiner[a], Achim Wixforth [a,b] and Christoph Westerhausen [a,b,c]

Experimental

S_{21} transmission signal measurement

To characterize the SAW chip and to check whether the thin catalyst layer possibly alters the SAW propagation mode, we manufactured two otherwise nominally identical SAW delay lines with and without the thin catalyst layer, which is shown in Fig. 1. The geometric structure of these IDTs are the same as the one used for acoustic-catalytic reaction, so the resonance frequency of them is also around 150MHz, the area of the catalyst layer is also kept as 2mm×8mm. Their rf transmission functions S_{21} are measured and compared employing a network analyzer. We measured the S_{21} transmission in the time domain (from 0 to 0.6µsec) as a function of frequency from 50MHz to 800MHz. This way, we are able to quite easily distinguish different acoustic modes. The result is shown in Fig. 2.

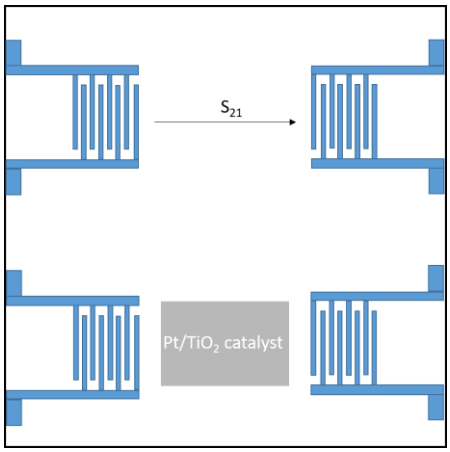

Fig. 1 structure of SAW device with two identical delay lines, one is without catalyst on the delay line and the other is with Pt/TiO_2 catalyst nanoparticle layer on the delay line.

Monitoring temperature changes and resonance frequency shifts

One might argue that the increase in formaldehyde production, indicating H_2 production in the photocatalytic process is due to an increased reaction temperature while the SAW is present. Moreover, the temperature is also critical for the resonance frequency of the IDT. Thus, temperature variation and shifts of the resonance frequency were investigated experimentally. A custom-made tiny temperature sensor was attached to the cylinder reaction chamber. Silver conductive paste was used to fill the gap between the sensor and the chamber. The temperature was recorded during the whole two photocatalytic reaction processes, 30min in dark and 60min under UV illumination, with and without applied SAW with a power level of P_{SAW}=40mW. The temperature change is shown in Fig. 2 and the resonance frequency shift and calculated output SAW energy at 150.3MHz is illustrated in Table. 1.

Monitoring hydrogen evolution using mass spectrometry

A mass spectrometer (Hyden Analytical HAL 201 RC) was coupled to the micro chamber outlet using a cold trap. The partial pressure of hydrogen was logged while the UV illumination was periodically switched on and off during the experiment.

[d] *Experimental Physics I, Institute of Physics, University of Augsburg, Germany*
[e] *Center for NanoScience (CeNS), Ludwig-Maximilian-University, Germany*
[f] *Physiology, Institute of Theoretical Medicine, University of Augsburg, Germany*

Results

SAW Transmission

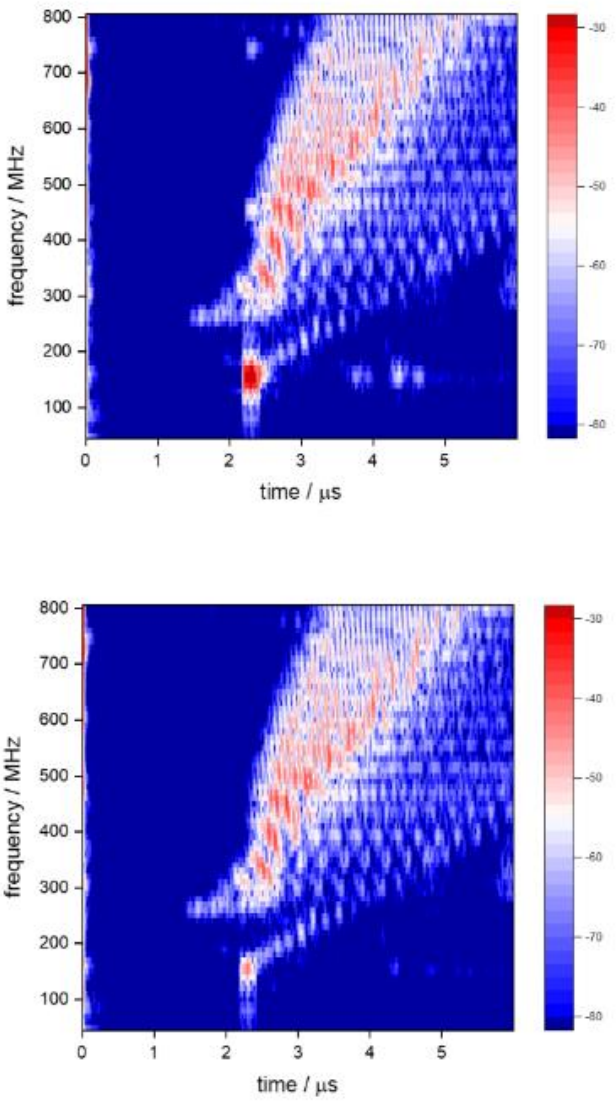

Fig. 2 transmission signal S_{21} at different frequencies in the time domain, the upper graph shows the experiment with no catalyst deposited on the delay line and the lower graph shows the experiment with catalyst on the delay line. The scale bar shows the scale of the S_{21} signal in dB.

Basically, two acoustic modes and a few echoes are seen in Fig. 2: The one with the largest signal (red) at f=150.3MHz and Δt= 2.3µsec represents the Rayleigh SAW, since the velocity of the surface acoustic wave is 3980m/s and the length of delay line is 8.7mm, so the propagation time of the surface acoustic wave from one IDT to the other IDT is around 2.3µs. In the upper graph, where no catalyst is present on the delay line, the S_{21} signal at 150.3MHz and 2.3µs is stronger than the S_{21} signal in right picture at same frequency and same time. This can be understood by the elastic and electric properties of the TiO_2 catalyst film that attenuates the S_{21} signal. The other S_{21} signal above 280MHz which exhibits a large slope results from bulk waves. These bulk waves are excited from the transducers directly. Comparing these two pictures, we can see that except a little damping (around 10dB) at the resonance frequency 150.3MHz and Δt=2.3µs, there is no other obvious difference between the two measurements. This indicates that the catalyst film on the delay line, most likely does not generate any other type of acoustic wave. When the power was applied to the IDT, a certain high percentage thereof will convert into a surface acoustic wave, with most of the acoustic energy being confined to the surface of $LiNbO_3$ and being able to interact and affect the combined catalyst film. The area of the nanoparticle film was kept around 2mm×8mm, and even though the catalyst causes attenuation, the surface acoustic wave could still pass through the whole catalyst film and reaches the opposite IDT. This also demonstrates that the whole catalyst film was affected by SAW.

Temperature Measurement

Fig. 3 shows the temperature change as a function of time. From 0 to 30 minutes, the UV light was turned off, so the recorded temperature is around room temperature (22.5°C). From 30 minutes to 60 minutes, the UV illumination and the SAW have been turned on, and the temperature increased immediately. As can be seen, both curves (UV only and UV plus 40mW SAW) are nearly identical. Thus, the temperature increase of about 20 K obviously is mainly caused by the UV illumination and the SAW with a power level of P_{SAW}=40mW cause a negligible additional temperature rise. Thus, it is safe to state that the SAW at power of 40mW, which clearly produces a doubling in the catalytic efficiency, does not act via an additional temperature increase but rather via intrinsic SAW related effects.

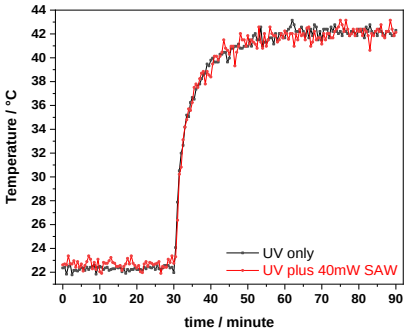

Fig. 3 Temperature change during the photocatalytical reaction process. From 0 to 30minutes, the UV light was off, then the UV illumination was turned on from 30 minutes to 60 minutes. the temperature increase has been measured (black trace). For comparison, the exact same experiment was performed but with the P_{SAW} = 40mW acoustic wave been turned on (red trace). The traces for SAW off and SAW on are nearly identical, indicating that the SAW does not alter the temperature during the experiment. The overall increase is thus mainly caused by the UV illumination.

To estimate the effect of the changing temperature on the SAW resonance frequency $f_{SAW} = v_{SAW} / \lambda_{SAW}$ during the experiment, we separately measured the SAW resonance frequency as a function of temperature, using a network analyzer (see Table 1). As v_{SAW} is known to be temperature dependent, we also expect f_{SAW} to change during the course of the experiment.

Table.1 SAW resonance frequency due to the temperature change during the photocatalytic experiment

time	T	Measured f_{SAW}	S_{11} at 150.34 MHz	Output SAW power/ input power
After 30min (dark)	22.5 °C	150.34 MHz	-8.98 dB	87.35%
After 30min (UV)	41.1 °C	150.16 MHz	-8.94 dB	87.24%
After 60min (UV)	42.3 °C	150.11 MHz	-8.92 dB	87.18%

The temperature coefficient for 128° rotated y-cut $LiNbO_3$ is 76ppm/°C.[1] Thus, we expect a change of f_{SAW} by about Δf_{SAW}=11.4KHz for every degree of temperature change.

In Table. 1, we show that the temperature increase after one hour illumination turned out to be almost ΔT =20 °C (see also Fig. 3), and the resonance frequency shifted by Δf_{SAW} = -240MHz which nicely agrees with the expected value. During the experiment and over the one hour illumination time, however, we kept the output frequency of the rf generator constant at 150.3MHz. This in turn is equivalent to a slight change of the SAW power, being caused by the temperature induced shift of f_{SAW}. This slight decrease of the SAW power can be estimated once the frequency dependent transmission function S_{12} or the power reflection S_{11} of the IDT is known. In Fig. 9, we show the measured S_{11} of the emitting IDT as a function of the frequency. As we can see, the temperature dependent Δf_{SAW} = -0.24MHz would result in only a very small power change which is estimated to be less than 0.1dB for the for ΔT= +20° being caused by the UV illumination. Hence, the observed nearly 100% increase of the catalytic efficiency due to SAW interaction might even be a bit larger, taking the non-compensated shift of the SAW resonance frequency into account.

Reference Measurement on glass

Fig. 4 shows the fluorescence spectra of reference measurements with the identical catalyst on a glass substrate. The preparation of the catalyst was done in the same way as for the samples. However, due to the process it is not possible to ensure the presence of the exact same amount of catalyst.

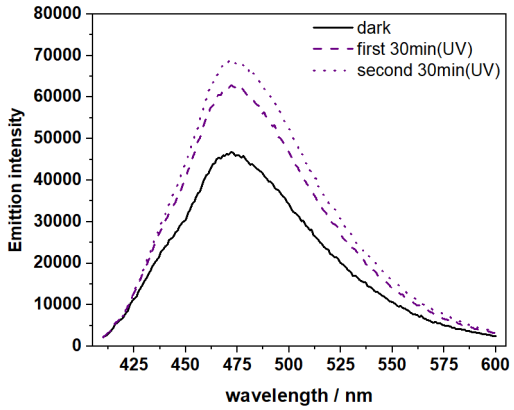

Fig. 4 Fluorescence emission intensity of the adsorption solution after 30 minutes in the dark (black line), after first 30minutes UV illumination of catalyst on glas without SAW (dashed line), and another 30minutes UV illumination without SAW (dotted line)

This results in an amount of produced formaldehyde of about 0.012 µmol. The enhanced activity compared to the reference on $LiNbO_3$ most likely is caused by preparation uncertainties.

Mass spectrometry

Fig. 5 shows the partial pressure of hydrogen in a reference experiment with SAW-application (40 mW). A mass spectrometer with a nitrogen cold trap was connected to the outlet of the reaction chamber. In contrast to the other shown experiments pure nitrogen was used as carrier gas. During the experiment the UV illumination was periodically switched on and off. As can be seen from the partial pressure as function of time, and its time derivative a clear correlation between illumination and detected hydrogen can be seen. This allows for the conclusion that we indeed observe water splitting here.

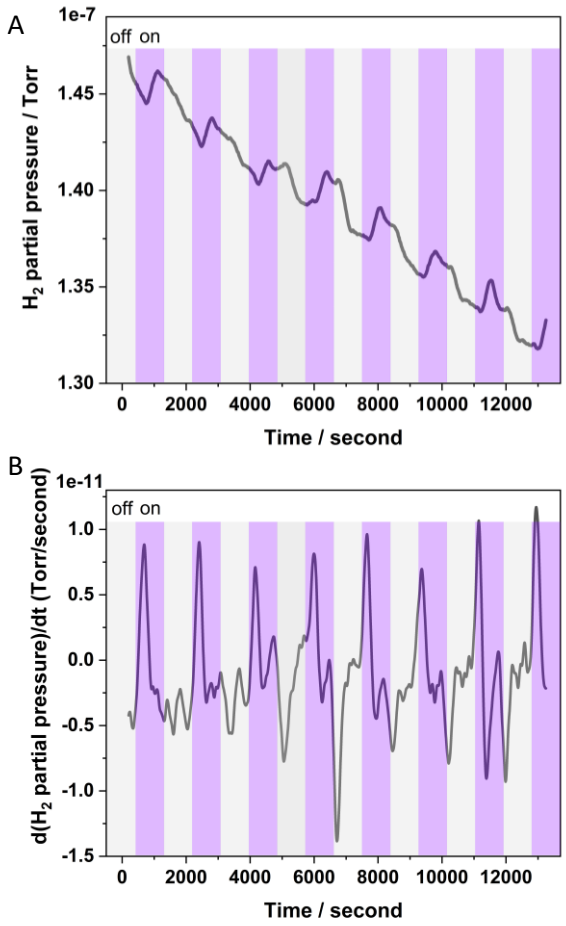

Fig. 5 A) Partial hydrogen pressure as function of time (UV on and off, SAW 40 mW). B) Time derivative of the data in A).

References

1 N. Dewan, M. Tomar, V. Gupta and K. Sreenivas, *Appl. Phys. Lett.*, 2005, **86**, 223508.

2